Anomalous Refraction in All-Dielectric Metagratings: The Finite Versus the Infinite Model

Cristina Ponti and Nikolaos L. Tsitsas

Abstract – All-dielectric metagratings are considered, which are composed of two alternating materials and exhibit significant anomalous refraction. The optimal parameters for their efficient operation have already been determined by a rigorous integral equation method applied to the infinitely periodic structure. In this work, we seek to determine the sufficient length (sufficient number of inclusions) so that the anomalous refraction effects are stabilized and become clearly visible in the corresponding finite metagratings. Numerical results are reported for three different gratings, investigating the variations of the induced fields with respect to the overall length of each structure. It is shown that, particularly in the region below the central cells, only a small number of inclusions is needed for obtaining the desired refracted fields.

1. Introduction

Metasurfaces enable new possibilities for manipulating wavefronts, paving the way for novel devices and applications [1, 2]. In traditional metasurfaces, a control of the amplitude and phase of the impinging beam is performed via a continuous and fast varying gradient of the surface impedance. Their realization is obtained with a large number of unit cells in the form of printed dipoles. Among the possible implementations, metasurfaces may be realized as metagratings, with important advantages in almost-unit steering of radiation and ease of realization [3–6]. The employed metagratings consist of fully dielectric arrays, in which carefully engineered dielectric inclusions are periodically embedded in a dielectric background. Manipulation of the impinging beam may provide anomalous reflection or refraction in directions not predicted by the conventional Snell's law [7, 8]. These effects may be exploited to improve the coverage of wireless links, especially at high frequencies, thanks to the low losses of the participating dielectric inclusions [9, 10]. Other interesting applications include lenses [11], power splitters [12], and retroreflectors [13].

The numerical modeling of all-dielectric metagratings is performed by various methods, which usually refer to infinitely periodic structures (i.e., periodic arrangements of infinite dielectric inclusions in a host medium) [14]. The main reason is that in infinitely periodic structures, Floquet's theorem applies, and the boundary-value problem is reduced to the basic unit cell. Established integral-equation approaches for infinite structures concern boundary- and volume-integral-equation methods [15–20], the method of analytical regularization [21, 22], the extended boundary condition method [23, 24], and the method of auxiliary sources [25, 26].

In practical implementations and in experimental realizations, the actual number of inclusions (elements) in the considered periodic configurations is crucial. Hence, when a method is applied to the solution of the associated boundary-value problem for an infinite structure, the conclusions on the occurrence of interesting physical phenomena need to be supplemented by selecting a sufficient number of inclusions so that the predicted phenomena are actually observable in practice. In this work, we conduct a relevant numerical investigation of all-dielectric metagratings, which have already been shown to provide significant anomalous refraction when considered and analyzed as infinite-periodic structures. We study the corresponding finite counterpart of each infinite metagrating, aiming to address the selection of a sufficient number of cells so that the finite structure exhibits effectively the same phenomena as the infinite one. The presented numerical results correspond to three distinct wavelengths in the visible range and to different types of constituent materials in the unit cell of the metagrating. Three different grating configurations are examined with small and high refraction-index contrasts between the inclusions and the background.

2. Formulation of the Problem

The infinitely periodic metagrating and its finitely periodic counterpart of length L are depicted in Figure 1. The Λ-periodic metagrating is illuminated by an E-polarized (TM_y-polarized) incident plane wave whose wavevector forms an angle of incidence θ with respect to the negative z-axis. The two adjacent dielectric materials, composing the unit cell, have refractive indices n_1 and n_2 and common thickness w. The duty cycle of the material with refractive index n_2 is denoted by s, so that inside the unit cell, the width of this material is $s\Lambda$, hence the width of the material with refractive index n_1 is $(1-s)\Lambda$. The external region is vacuum with a refractive index of n_0. The configuration is uniform along y with constant magnetic permeability. The infinitely periodic metagrating (Λ-periodic with respect to the x-axis) is depicted in Figure 1a. Its finite

Manuscript received 9 October 2025.

Cristina Ponti is with the Department of Industrial, Electronic and Mechanical Engineering, Roma Tre University, Rome, Italy; e-mail: cristina.ponti@uniroma3.it.

Nikolaos L. Tsitsas is with the School of Informatics, Aristotle University of Thessaloniki, Thessaloniki, Greece; e-mail: ntsitsas@csd.auth.gr.

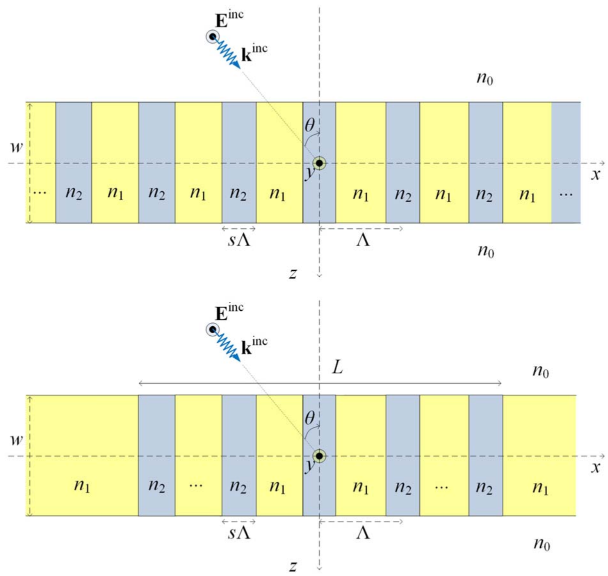

Figure 1. Two-dimensional layouts of the considered (a) infinitely periodic and (b) finitely periodic metagratings.

counterpart is a slab of refractive index n_1 and thickness w hosting a finite and odd number N of inclusions with the same thickness and refractive index n_2. Thus, the finitely periodic metagrating has Λ-periodic cells of total length L (see Figure 1b).

Diffraction by the infinitely periodic metagrating of Figure 1a is modeled efficiently by volume-integral-equation methods. Here, we employ the second-kind Fredholm integral equation method developed in [19] and [20]. In this method, the unknown function is the electric field in the inclusion regions. The involved volume integral equation is discretized using an entire-domain Galerkin technique, leading to a nonhomogeneous algebraic system for the Fourier series coefficients of the unknown electric field. The developed semianalytical algorithm is characterized by guaranteed convergence and provides high accuracy, which is easily controlled by the order of discretization.

On the other hand, volume-integral-equation methods, like the above-mentioned ones, cannot be directly applied for the analysis of scattering by the finitely periodic configuration of Figure 1b. This is because in the finite case, the problem cannot be reduced to a single unit cell. Moreover, the spectral-domain expression of the (background) layered-medium Green's function can no longer be appropriately exploited and processed via Poisson's summation formula. To this end, for the analysis of the finite metagrating, we perform the relevant field simulations using a commercial general-purpose electromagnetic software package, as described in detail below.

3. Numerical Results

Consider metagratings of the form shown in Figures 1a or 1b, specifically designed to generate significant anomalous refraction. This means that the structures are optimized to support maximum refracted power P^t_{-1} in the -1 order, whereas the powers P^r_{-1} of the 1-reflected, P^r_0 of the 0-reflected and P^t_0 of the 0-refracted orders remain as close to zero as possible. Hence, almost-unit steering of the incident wave to the antisymmetric refracted direction is obtained, leading to anomalous (negative) refraction below the metagrating.

We start with the infinite metagrating of Figure 1a and exploit the designs of [8] derived by the volume-integral-equation approach of [19] and [20]. For the optimizations, the main degrees of freedom were w, s, and Λ. We use the optimal input parameters resulting from the operation of the infinite metagrating achieving anomalous refraction to examine the performance of the corresponding finite structure of length L depicted in Figure 1b. The scattered field from the finite metagrating is evaluated using a general-purpose electromagnetic solver. We are interested in testing numerically how and to what extent the fields scattered from the finite metagratings approach those diffracted from the corresponding infinite ones as the length L (or equivalently, the number N of inclusions) increases. Such numerical tests enable us to address how large need finite metagratings realistically be so as to support, with a good approximation, anomalous refraction already predicted from the corresponding infinite configurations.

First, a finite metagrating is considered with vacuum inclusions in hafnium dioxide (HfO_2) background with refraction index $n_1 = 2.1$. The corresponding infinite structure was optimized at the green wavelength $\lambda_0 = 530$ nm using the approach outlined in Section 2. The optimal parameters were found to be $w = 174$ nm, $\Lambda = 678$ nm, and $s = 0.66$, at an incidence angle $\theta = 24^\circ$ [8]. This optimized layout delivers $P^t_{-1} = 92\%$ in the -1-refracted order in the direction $\theta_{-1} = 22^\circ$, with respect to the positive z-axis. For the numerical simulations of the finite metagrating in CST Microwave Studio [27], the structure was modelled as a two-dimensional (2D) layout, with a limited and small thickness, shorter than $\lambda_0/10$ along y. The boundaries embedding the layout on the xz-planes are perfect electric conductors, forcing an infinite extension of the structure along y with a polarization of the electric field of the impinging wave parallel to the y-axis. A hexahedral mesh type is used, with a decomposition into 20 cells per wavelength, applied both to the metagrating and to the vacuum region far from the structure. At the edges of the domain, PML boundaries are imposed, fixed at a minimum distance to the structure of $\lambda_0/4$, with an estimated reflection level of 0.0001.

For the finite metagrating, a structure with a sufficiently large number of inclusions, providing a stable and convergent result in the central cells, was initially considered. After extensive numerical tests, it was found that $N = 31$ inclusions offer such stable and convergent fields, also coinciding with the fields obtained by the integral-equation approach of [19] for the infinite

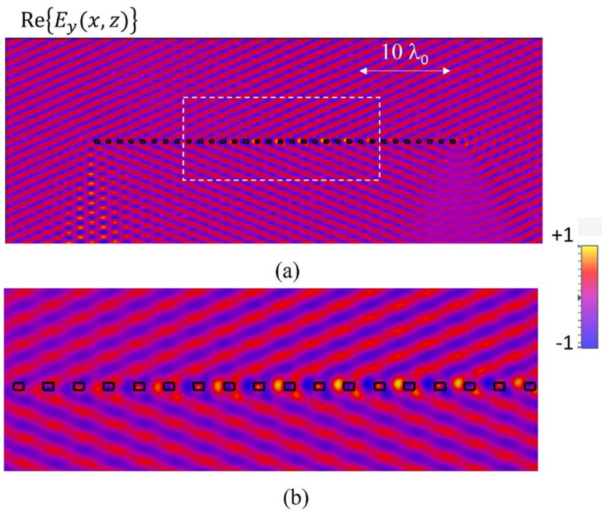

Figure 2. (a) Real part of $E_y(x,z)$ at the green wavelength ($\lambda_0 = 530$ nm) for a finite metagrating with $N = 31$ inclusions, (b) zoomed-in distribution in the region of the central cells (included in the dotted white box in [a]).

grating. The 2D color map of the real part of $E_y(x,z)$ for $N = 31$ is shown in Figure 2. Anomalous refraction of the wavefront is clearly visible, as well as the almost unitary transmission below the periodic structure.

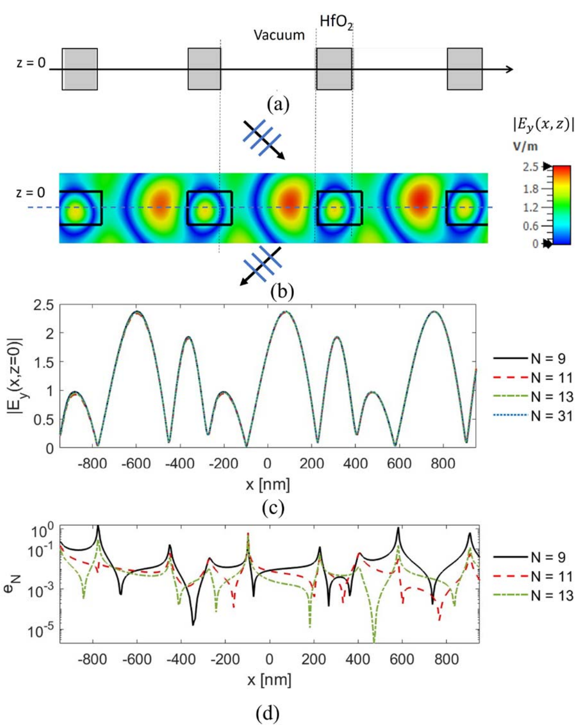

Figure 3. Green wavelength ($\lambda = 530$ nm): (a) the central cells for the HfO_2/vacuum metagrating; (b) 2D colormap of the magnitude of the electric field in the central cells of (a) for a long metagrating with $N = 31$; (c) plot of the magnitude of the electric field along $z = 0$, for increasing N; (d) relative errors e_N between the fields for the considered N and the reference solution (for $N = 31$).

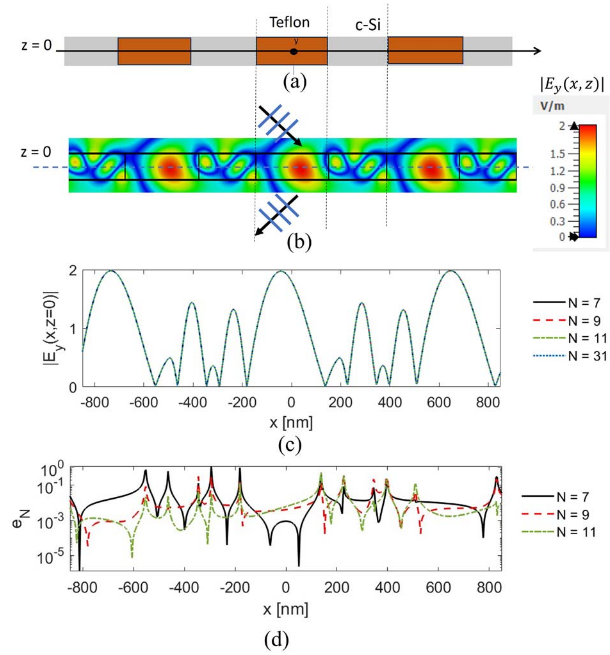

Figure 4. Orange wavelength ($\lambda = 610$ nm): (a) the central cells for the Teflon/c-Si metagrating; (b) 2D colormap of the magnitude of the electric field in the central cells of (a) for a long metagrating with $N = 31$; (c) plot of the magnitude of the electric field along the line $z = 0$, for increasing N; (d) relative errors e_N between the fields for the considered N and the reference solution (for $N = 31$).

Next, we further study the interaction between the incident plane wave and the considered HfO_2/vacuum finite metagrating (see Figure 3a). We investigate the variations in the fields in the central cells to see how they approach those in Figure 2 as N increases from small values to $N = 31$. In Figure 3b, the plot of $|E_y(x,z)|$ is zoomed across the three central cells, for the same structure as in Figure 2. A peak field appears in the vacuum inclusions, while the HfO_2 inclusions, as a denser medium, provide the needed phase delay for the anomalous refraction of the field at the interface with the lower vacuum half space. In Figure 3c, the magnitude of the electric field is plotted along the line $z = 0$, internal to the metagrating, as a function x for finite structures with different numbers N. A stable pattern is observed, which converges rapidly to the reference solution already for a small N; the reference solution corresponds to $N = 31$ simulated in Figure 2. The fast convergence is also demonstrated in Figure 3d by the small relative errors e_N between the fields for the considered N and the reference solution (for $N = 31$).

The second case concerns a metagrating with a high refraction-index contrast. The material used in the background is crystalline Silicon (c-Si), having a dispersive refraction index n_1 obtained from [28], whereas the material of the inclusion belongs to nondispersive Teflon AF fluoropolymers with a constant refractive index of $n_2 = 1.3$. With the wavelength selected at the orange color (i.e., $\lambda_0 = 610$ nm), optimization of the

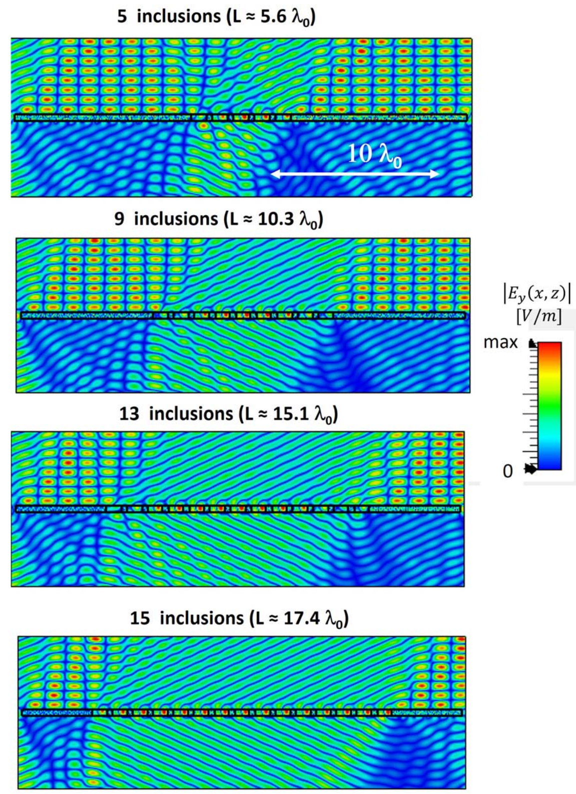

Figure 5. Blue wavelength (λ_0 = 470 nm): magnitude of the electric field $E_y(x,z)$ for increasing numbers N of inclusions of the c-Si/Teflon metagrating.

infinite structure yields w = 138 nm, Λ = 691 nm, and $s = 0.56$, for $\theta = 26^\circ$ [8]. At λ_0 = 610 nm, for c-Si, $n_1 = 3.93$ [28]. The 2D color map of $E_y(x,z)$ in the Teflon/c-Si finite structure with $N = 31$ was obtained and found to be very similar to that of Figure 2. Hence, this is the reference solution for this case, offering stabilized fields exhibiting anomalous refraction below the metagrating. The layout of the Teflon/c-Si metagrating is shown in Figure 4a. The zoomed spatial distribution of $|E_y(x,z)|$ across the three central cells is depicted in Figure 4b. The magnitude of the field along the line $z = 0$ versus x for increasing N is plotted in Figure 4c, while the relative error e_N between the fields for the considered N and the reference solution is shown in Figure 4d. The conclusions from Figure 4 for the orange color are similar to those from Figure 3 for the green color. In fact, for the orange color, the field pattern in the central cells converges even faster (i.e., $N = 11$ is sufficient for small errors e_N).

The third case is an additional example of a high-refraction-index contrast structure, now considered at the blue wavelength of $\lambda_0 = 470$ nm. The constituent materials are again c-Si and Teflon. The optimal parameters of the infinite structure were determined as $w = 180$ nm, Λ = 557 nm, and $s = 0.72$, for $\theta = 25^\circ$, and an angle of diffraction in the -1-refracted order $\theta_{-1} = 25^\circ$ [8]; hence, the anomalous refraction direction is exactly antisymmetric with the angle of incidence. A long, but finite-length metagrating was simulated, yielding a 2D field map very similar to that of Figure 2. The number of inclusions considered was $N = 31$. This corresponds to a total length of the structure comparable to the map simulated in Figure 2a of [8], showing a practically unitary transmission of the wavefront below the grating layer, in the anomalous direction of refraction (i.e., along the direction of the angle $\theta_{-1} = 25^\circ$). The prediction from the infinite model was that the refracted power in the -1-order is $P^t_{-1} = 99\%$; hence, almost the entire incident field's power is transmitted in the -1-order below the periodic layer. Plots of $E_y(x,z)$ as N increases are shown in Figure 5. The number of cells below which the anomalous refraction effect is clearly visible increases quickly with N. In the region below the central cells, the refracted field is stabilized quickly. In that region, even $N = 9$ is sufficient for converged and strong anomalous refraction.

4. Conclusions

All-dielectric metagratings of two alternating materials were investigated. Such infinitely periodic structures have already been optimized to exhibit anomalous refraction via a volume-integral-equation approach. Here, we considered the corresponding finitely periodic counterparts and examined the diffracted fields for an increasing number of inclusions. It was shown that the stabilization of the fields, showcasing anomalous refraction, requires only a small number of inclusions, especially below the central cells. This could prove useful when the refracted fields are required in a limited spatial region without resorting to unnecessarily long gratings.

References

1. C. L. Holloway, E. F. Kuester, J. A. Gordon, J. O' Hara, J. Booth, et al., "An Overview of the Theory and Applications of Metasurfaces: The Two-Dimensional Equivalents of Metamaterials," *IEEE Antennas and Propagatation Magazine*, **54**, April 2012, pp. 10-35.
2. S. B. Glybovski, S. A. Tretyakov, P. A. Belov, Y. S. Kivshar, and C. R. Simovski, "Metasurfaces: From Microwaves to Visible," *Physics Reports*, **634**, May 2016, pp. 1-72.
3. Y. Ra'di, D. L. Sounas, and A. Alù, "Metagratings: Beyond the Limits of Graded Metasurfaces for Wave Front Control," *Physical Review Letters*, **119**, Aug. 2017, p. 067404.
4. Y. Ra'di and A. Alù, "Metagratings for Efficient Wavefront Manipulation," *IEEE Photonics Journal*, **14**, February 2022, p. 2207513.
5. A. Epstein and O. Rabinovich, "Unveiling the Properties of Metagratings via a Detailed Analytical Model for Synthesis and Analysis," *Physical Review Applied*, **8**, November 2017, p. 054037.
6. O. Rabinovich and A. Epstein, "Arbitrary Diffraction Engineering With Multilayered Multielement Metagratings," *IEEE Transactions Antennas Propagation*, **68**, Mar. 2020, pp. 1553-1568.
7. N. L. Tsitsas and C. A. Valagiannopoulos, "Anomalous Reflection of Visible Light by All-Dielectric Gradient

Metasurfaces," *Journal of the Optical Society of America B*, **34**, July 2017, pp. D1-D8.

8. N. L. Tsitsas and C. Valagiannopoulos, "Anomalous Refraction Into Free Space With All-Dielectric Binary Metagratings," *Physics Review Research*, **2**, Sep. 2020, p. 033526.
9. S. Ceccuzzi, P. Baccarelli, C. Ponti, and G. Schettini, "Effect of Source Position on Directive Radiation in EBG Structures With Epsilon-Near-Zero Behavior," *IEEE Antennas and Wireless Propagation Letters*, **18**, June 2019, pp. 1253-1257.
10. C. Ponti, P. Baccarelli, S. Ceccuzzi, and G. Schettini, "Tapered All-Dielectric EBGs With 3-D Additive Manufacturing for High-Gain Resonant-Cavity Antennas," *IEEE Transactions Antennas Propagation*, **69**, May 2021, pp. 2473-2480.
11. S. Zhang, C. Li, L. Ke, B. Fang, J. Lu, et al., "All-Dielectric Terahertz Wave Metagrating Lens Based on 3D Printing Low Refractive Index Material," *Infrared Physics Technology*, **133**, September 2023, p. 104775.
12. J. Wang, "Polarization Beam Splitter Empowered by a Two-Dimensional Diffraction Metagrating," *Journal of the Optical Society of America B*, **42**, April 2025, pp. 693-699.
13. M. Li, L. Jing, X. Lin, S. Xu, L. Shen, et al., "Angular-Adaptive Spin-Locked Retroreflector Based on Reconfigurable Magnetic Metagrating," *Advanced Optical Materials*, **7**, July 2019, p. 1900151.
14. N. L. Tsitsas, "Integral-Equation Methods for All-Dielectric Gratings," *Philosophical Transactions of the Royal Society A*, **383**, August 2025, 20240340.
15. D. Maystre and E. Popov, "Integral Method for Gratings," in E. Popov (ed.), *Gratings: Theory and Numeric Applications*, Marseille, Institut Fresnel, Université d'Aix-Marseille, CNRS, 2012, pp. 4.1–4.55.
16. L. I. Goray and G. Schmidt, "Solving Conical Diffraction Grating Problems With Integral Equations," *Journal of the Optical Society of America A*, **27**, March, 2010, pp. 585-597.
17. A. Sentenac and J. J. Greffet, "Scattering by Deep Inhomogeneous Gratings," *Journal of the Optical Society of America A*, **9**, June 1992, pp. 996-1006.
18. M. Paulus and O. J. F. Martin, "Green's Tensor Technique for Scattering in Two-Dimensional Stratified Media," *Physical Review E*, **63**, May 2001, p. 066615.
19. N. L. Tsitsas, D. I. Kaklamani, and N. K. Uzunoglu, "Rigorous Integral Equation Analysis of Nonsymmetric Coupled Grating Slab Waveguides," *Journal of the Optical Society of America A*, **23**, November 2006, pp. 2888-2905.
20. N. L. Tsitsas, "Second-Kind Fredholm Integral-Equation Analysis of Scattering by Layered Dielectric Gratings," *IET Microwaves Antennas and Propagation*, **15**, May 2021, pp. 1194-1205.
21. D. M. Natarov, V. O. Byelobrov, R. Sauleau, T. M. Benson, and A. I. Nosich, "Periodicity-Induced Effects in the Scattering and Absorption of Light by Infinite and Finite Gratings of Circular Silver Nanowires," *Optics Express*, **19**, October 2011, pp. 22176-22190.
22. V. O. Byelobrov, T. M. Benson, and A. I. Nosich, "Binary Grating of Subwavelength Silver and Quantum Wires as a Photonic-Plasmonic Lasing Platform With Nanoscale Elements," *IEEE Journal of Selected Topics in Quantum Electronics*, **18**, November 2012, pp. 1839-1846.
23. W. N. Cain, V. K. Varadan, V. V. Varadan, and A. Lakhtakia, "Reflection And Transmission Characteristics of a Slab With Periodically Varying Surfaces," *IEEE Transactions Antennas Propagation*, **AP-34**, September 1986, pp. 1159-1163.
24. A. Lakhtakia, V. K. Varadan, and V. V. Varadan, "Excitation of Layered Media Having Rough Interfaces by Line Sources," *IEEE Transactions Antennas Propagation,* **AP-35**, April 1987, pp. 462-466.
25. A. Boag, Y. Leviatan, and A. Boag, "Analysis of Two-Dimensional Electromagnetic Scattering From Nonplanar Periodic Surfaces Using a Strip Current Model," *IEEE Transactions Antennas Propagation*, **37**, November 1989, pp. 1437-1446.
26. A. Ludwig and Y. Leviatan, "Analysis of Bandgap Characteristics of Two-Dimensional Periodic Structures by Using the Source-Model Technique," *Journal of the Optical Society of America A*, **20**, August 2003, pp. 1553-1562.
27. SIMULIA, "CST Studio Suite," https://www.3ds.com/products/simulia/cst-studio-suite.
28. RefractiveIndex.Info, "Refractive Index Database," http://refractiveindex.info/ (Accessed 30 March 2025).